Versi Online: http://journal.ipb.ac.id/index.php/jtip
https://doi.org/10.6066/jtip.2026.37.2.157
Research Article

Jurnal Teknologi dan Industri Pangan/Journal of Food Technology and Industry
Vol. 37(2): 157-170 Th. 2026 ISSN: 1979-7788
Terakreditasi Kemdiktisaintek: 295/C/C3/KPT/2026

Effect of Particle Size on the Physical Properties of Red Ginger (*Zingiber officinale* var. *rubrum*) Powder

Siti Aminah[1,2], Nancy Dewi Yuliana[1)], Eko Hari Purnomo[1)], Etik Mardliyati[3)], Purwiyatno Hariyadi[1)]*

[1)] Division of Food Science and Technology, Faculty of Engineering and Technology, IPB University, Bogor, Indonesia
[2)] Department of Food Technology and Nutrition, Faculty of Halal Food Science, Djuanda University, Bogor, Indonesia
[3)] Research Center for Vaccine and Drug, National Research and Innovation Agency (BRIN), Indonesia

Received January 8th 2026 / Revised May 21st 2026 / Accepted June 9th 2026

ABSTRACT

This study investigated the effect of particle size on the physical properties of red ginger (*Zingiber officinale* var. *rubrum*) powder. The parameters analyzed included flow characteristics (bulk density, tapped density, Hausner ratio, compressibility index, and angle of repose), water content, water solubility, color, and morphology. Red ginger powder (RGP) samples were prepared across the millimeter-to-nanometer particle-size range with D_{50} values of 2256, 2066, 636, 580, 47.38, 40.37, 39.98, 34.82, and 0.22 μm. As the results, the particle size of RGP decreased from coarse (D_{50} 2256 μm) to fine (D_{50} 40.37–34.82 μm). While the bulk density fluctuated (0.32–0.34 g/cm³), the tapped density increased consistently (0.36–0.56 g/cm³). This increase in density was accompanied by rises in the Hausner ratio (1.12–1.73), compressibility index (10.77–42.17%), and angle of repose (22.98–39.71°). However, when the particle was further reduced to the nanopowders (D_{50} 0.22 μm), the Hausner ratio, compressibility index, and angle of repose slightly decreased to 1.54, 34.95%, and 37.07°, respectively, which were lower than the values at D_{50} 34.82 μm. The reversal occurs because the agglomerates behave as larger particles, with cohesive van der Waals forces predominantly affecting them. Water solubility and color brightness (L*) increased significantly with decreasing powder particle size, from 19.64 to 31.65% and from 27.9 to 55.4. Increase in surface area is thought to enhance solvent and light interactions. Water content increased from 10.51 to 15.06% as particle sizes decreased from 2256 to 47.38 μm, but decreased to 10.81% in nanopowders (D_{50} 0.22 μm), likely due to agglomeration that reduces the accessible surface area. Overall, this study revealed that particle size reduction improved the water solubility, brightness, and density of RGP, particularly on the nanoscale, highlighting particle size control as a critical factor in food product development.

Keywords: nanoparticle, particle size, powder properties, red ginger powder, water solubility

INTRODUCTION

Red ginger (*Zingiber officinale* var. *rubrum*) is a spice of commercial significance, traditionally utilized as both a medicinal component and a culinary spice. Red ginger contains higher levels of bioactive compounds, such as gingerol, shogaol, and zingerone, in comparison to other ginger cultivars (Badrunanto *et al.,* 2024). Transforming red ginger into powder significantly extends its shelf life, enhances transportability, and improves its utility in various culinary applications. Red ginger powder (RGP) is a natural flavoring and coloring agent in the food sector. This powder is a raw material for health supplements and phytopharmaceuticals in the pharmaceutical sector, attributed to its antioxidant, anti-inflammatory, anti-nausea, and antibacterial characteristics (Mao *et al.,* 2019).

The physicochemical properties of ginger powder affect its processing, storage, and end use. Among these properties, particle size has been identified as a key determinant (Camacho *et al.,* 2022). The increased surface area leads to deformation of the tissue structure. Other research reported that white ginger powder with particle sizes of 300, 149, 74, 37, and 8.34 μm exhibited densities and water solubility index (WSI) values that increased as particle size decreased (Shen *et al.,* 2023). However, the majority of investigations remain confined to the micrometer size range. Investigations on the impact of particle size throughout a broader range of sizes, especially at the nanoscale, on the physical properties of red ginger remain insufficient.

*Corresponding Author: E-mail: phariyadi@apps.ipb.ac.id

This study investigated the impact of particle size on RGP physical characteristics, including flow behavior (bulk density, tapped density, Hausner ratio, compressibility index, and angle of repose), moisture content, water solubility, color (L*, a*, b*, and ΔE), and morphology, covering particle sizes from the millimeter to the nanoscale range. The findings are expected to improve understanding of particle size's influence on the quality of RGP and support the development of spice-based functional food products.

MATERIALS AND METHOD

Materials

The materials utilized in this study consist of red ginger simplicia sourced from PT Palapa Muda Perkasa Depok, methanol (Merck, Germany), ethanol (Merck), aluminum cups, Whatman No. 42 filter paper, and zip-lock plastic bags.

Preparation of RGP

Rhizomes of red ginger were procured from the Palapa Muda Perkasa Plantation located in Bogor Regency, West Java. The red ginger rhizomes used were sourced from ginger plants that were 7 to 8 months old. The red ginger rhizomes were carefully cleaned, finely sliced, and subjected to oven-dried at 50–55 °C for approximately 40 h to obtain dried simplicia. RGP of varying particle sizes was produced utilizing three milling methods: a blender (HR2115, Philips, Guangdong, China), a dry food grinder (DFG; FCT-Z100, Fomac, Zhejiang, China), and a planetary ball mill (PBM; PM 200, Retsch, Haan, Germany). Coarse RGP was produced by grinding red ginger simplicia with a blender. Grinding durations ranged from 5 to 15 s. DFG was employed to acquire a more refined ginger powder. Grinding durations ranged from 15, 30, 60, 120, to 300 s, with 60 s grinding intervals succeeded by a 5-min rest period. Nano-sized RGP was synthesized utilizing PBM. A 2 g of powder from DFG grinding for 300 s was placed into a PBM with 2 mm alumina beads, ensuring that the volume did not surpass two-thirds of the jar's capacity. The sample was ground for 10–30 s (on) and 10–30 min (off) for 12–20 h at 300–700 rpm speed. The resultant RGP was subsequently stored in an airtight plastic bag at a temperature of approximately −18 °C until analysis.

Particle size and morphology

The particle size characterization of RGP was conducted utilizing several methods. The methodologies and tools were tailored to the anticipated particle size range of the powder. The powder, processed with a blender for 5, 10, and 15 s, along with DFG for 15 s, was evaluated using the sieve method (Biazzi *et al.,* 2022). The powder, ground with DFG for durations of 30, 60, 120, and 300 s, was evaluated via the laser diffraction (LD) method (Laser Particle Sizer; LLPA-C10, Labtron Equipment Ltd., Camberley, United Kingdom) at a temperature of 25±1.0 °C, for 50 s, within a measurement range of 0.1–2000 *µ*m (Permanadewi *et al.,* 2022). The powder milled using PBM was examined utilizing the dynamic light scattering (DLS) technique with a Malvern Zetasizer Pro (ZSU 3200, Malvern Panalytical Limited, Malvern, United Kingdom). The scanning electron microscope (SEM) (JEOL JSM-6510LA, JEOL Ltd., Akishima, Tokyo, Japan) was operated at 20 kV, and ImageJ (National Institutes of Health, Bethesda, Maryland, USA) was utilized to ascertain the particle size and morphology of the powder.

Density

Bulk density (ρ_{bulk}) was determined by weighing approximately 2 g of the sample and placing it into a 10 mL measuring cylinder to record the volume. The bulk density was calculated by dividing the mass by the volume. The tapped density (ρ_t) is determined by tapping a measuring cylinder containing approximately 2 g of sample 100 times until the volume stabilizes, followed by calculating it as the mass divided by the final volume. The Hausner ratio (Equation 1) and compressibility index (Equation 2) are derived from the bulk density and tapped density readings.

$$\text{The Hausner Ratio} = \frac{\rho_t}{\rho_{bulk}} \quad \ldots\ldots\ldots\ldots (1)$$

$$\text{Compressibility Index} = \frac{(\rho_t - \rho_{bulk})}{\rho_t} \times 100 \quad \ldots\ldots\ldots\ldots (2)$$

The angle of repose is ascertained by gradually pouring approximately 5 g of the sample until a conical pile is created, followed by measuring the height (h) and the base radius (r). The angle of repose is then computed using the formula $\theta = \tan^{-1}(h/r)$ (Abel *et al.,* 2020). Flowability was classified based on the angle of repose according to the criteria established by Müller *et al.* (2021): 25–30° very free flowing; 30–38° free flowing; 38–45° fair flowing; 45–55° cohesive; and >55° very cohesive. The Hausner ratio (HR) and compressibility index (CI) were interpreted according to Carr (1965) and Hausner (1967). The classification criteria were as follows: HR <1.25 free flowing; 1.25–1.5 moderate flow; and >1.5 cohesive (Hausner, 1967); CI <10% excellent; 11–15% good; 16–20% fair; 21–25% passable; 26–31% poor; 32–37% very poor; and >38% very, very poor (Carr, 1965).

Moisture content

The moisture content of RGP was analyzed using the oven technique, utilizing 1 g of sample in a pre-dried and weighed aluminum cup. The sample was desiccated at approximately 105 °C for 5 h, subsequently cooled in a desiccator, and weighed until a stable weight (≤0.0005 g) was achieved. The weight difference determined the moisture content before and after drying.

Solubility

Water solubility of RGP was determined using the gravimetric method adapted from Cano-Chauca *et al.* (2005). A 0.5 g sample was weighed and dissolved in 100 mL of distilled water, then filtered using a vacuum filter with Whatman No. 42 filter paper. Prior to use, the filter paper was dried at 150 °C for 30 min and weighed. After filtration, the filter paper together with the residue was dried again in an oven at 150 °C for approximately 3 h, cooled in a desiccator for 15 min, and weighed. Weighing was repeated until a constant weight was obtained (≤0.0005 g). Water solubility was calculated using Equation 3.

$$\text{Water Solubility (\%)} = \frac{W_1-(W_3-W_2)}{W_1} \times 100 \quad \ldots\ldots\ldots\ldots (3)$$

W_1= the initial sample weight (g); W_2= the weight of the filter paper and residue after drying (g); W_3= the weight of the empty filter paper before filtration (g).

Color

Color analysis of RGP using digital colorimetric techniques (Weston *et al.,* 2020). The powder was compacted and positioned in a glass container at an equivalent height. Images were taken using a smartphone digital camera at 30 cm with a white background. Images were examined at five points of each sample using Adobe Photoshop CS3 (Adobe Systems Incorporated, America). RGB values were converted to CIELAB color space using D_{50} illuminant and 2° standard observer to obtain L*, a*, and b* values. The results obtained were transmitted to Microsoft Excel to calculate the average.

Data analysis

Data analysis was conducted at a 5% significance level using a completely randomized design (CRD). All measurements were performed in triplicate (n= 3). Statistical evaluation was performed with IBM SPSS statistics software (Version 25.0; IBM Corp., Armonk, New York, USA) through analysis of variance (ANOVA), followed by Duncan's multiple range test for post-hoc comparisons.

RESULTS AND DISCUSSION

Particle size distribution

It is essential to perform particle size analysis to understand the characteristics of powders (Dacanal, 2024). Several approaches are available to describe the size and shape of a powder. Different analytical methods will lead to different distributions of particle sizes (Islam *et al.,* 2022). Each method was selected based on its suitability for the expected particle size range of the analyzed samples. This was done because no single measurement technique provides accurate and representative results across the entire particle size spectrum from the millimeter to the nanoscale range (Islam *et al.,* 2022). Sieve analysis was applied to coarse ginger powder sample produced by blending for 5, 10, 15 s and DFG for 15 s. This method is well established for particles above 75 *μ*m, whereas particles smaller than 45 *μ*m may agglomerate during sieving, which causes sieve clogging and biased size estimates. LD was used for medium-sized DFG powders produced by grinding for 30–300 s, given its accuracy and repeatability in the micrometer range. DLS was used for nanoscale PBM powder, as DLS is specifically designed for particles in the sub-micrometer range (Jia *et al.,* 2023).

SEM (ImageJ) was applied to all sample types as a common complementary approach to evaluate particle morphology and relative trends of particle size reduction observed across treatments, consistent with recommendation in the literature (Roostaei *et al.,* 2020). However, SEM was not used as the sole primary method for particle size distribution analysis due to several considerations. First, the field of view captured in a single SEM image represents only a small portion of the total powder population, which may introduce bias, especially for samples with a broad particle size distribution (Whiting *et al.,* 2022). Second, SEM estimates particle size based on the longest diameter seen in a two-dimensional projection, which may not accurately reflect the true three-dimensional particle size, especially for the irregular and asymmetric morphologies characteristic of RGP. Third, for coarser powders with particle sizes in the range of hundreds to thousands of micrometers, the SEM field of view tends to capture only a limited number of large particles, thus not representing the overall size distribution of the powder (Roostaei *et al.,* 2020). Therefore, three measurement methods (sieving, LD, DLS) were used as the primary methods according to the relevants particle size range, while SEM analysis was used as a complementary validation approach.

The primary objective of this analysis was to evaluate how different grinding treatments (blender, DFG, and PBM) reduced the particle size of RGP across different size ranges. As shown in Table 1 and Figures 1 and 2, particle size decreased progres-

sively with increasing grinding intensity and duration across all treatments. The sieve method showed particle sizes ranging from several hundred to several thousand micro-meters for powders processed using a blender (t= 5, 10, 15 s) or a DFG (t= 15 s). However, this difference is in line with previous studies reporting that, for fine powders in the micrometer range, LD measured smaller values than SEM due to differences in measurement basis (Whiting *et al.,* 2022). LD, supported by SEM (ImageJ), was used to analyze DFG powders processed for longer durations (t= 30, 60, 120, and 300 s). These samples could not be assessed using the sieve method because particles smaller than 45 *μ*m tend to adhere and form agglomerates during sieving. Such agglomeration can "blind" the sieve, resulting in biased size estimates (Islam *et al.,* 2022). The LD method produced particle size distributions that were narrower and smaller than those obtained via SEM. This is because LD determines the equivalent spherical diameter using laser light scattering, allowing for more consistent measurement of fine particles.

Table 1. Particle size distribution of red ginger powder (RGP) produced by different milling methods and measured by various analytical techniques

Sample	Analysis method	D_{10} (*μ*m)	D_{50} (*μ*m)	D_{90} (*μ*m)	D_{av} (*μ*m)
Blender 5	Sieving	344.00	2256.00	5963.00	3673.00
	SEM	149.70	316.35	1016.10	431.70
Blender 10	Sieving	139.00	2066.00	3297.00	2155.00
	SEM	198.33	302.25	562.62	339.43
Blender 15	Sieving	88.00	580.00	2236.00	1115.00
	SEM	118.36	221.94	372.18	248.95
DFG 15	Sieving	88.00	636.00	2809.00	1059.00
	SEM	121.94	173.88	338.58	207.50
DFG 30	LD	25.83	47.38	86.83	53.02
	SEM	96.86	164.46	237.22	168.71
DFG 60	LD	21.26	39.98	75.13	45.16
	SEM	62.76	86.85	203.01	113.07
DFG 120	LD	21.55	40.37	75.59	45.54
	SEM	33.70	63.82	108.59	75.95
DFG 300	LD	18.10	34.82	66.93	39.67
	SEM	27.58	42.18	78.28	46.03
PBM	DLS	0.17	0.22	0.31	0.23
	SEM	0.11	0.17	0.54	0.23

Note: DFG= dry food grinder; PBM= planetary ball mill; LD= laser diffraction; DLS= dynamic light scattering; SEM= scanning electron microscopy. Numbers after Blender/DFG indicate grinding duration in seconds. D_{10}, D_{50}, D_{90}= particle diameters below which 10%, 50%, and 90% of particles fall; D_{av}= average diameter

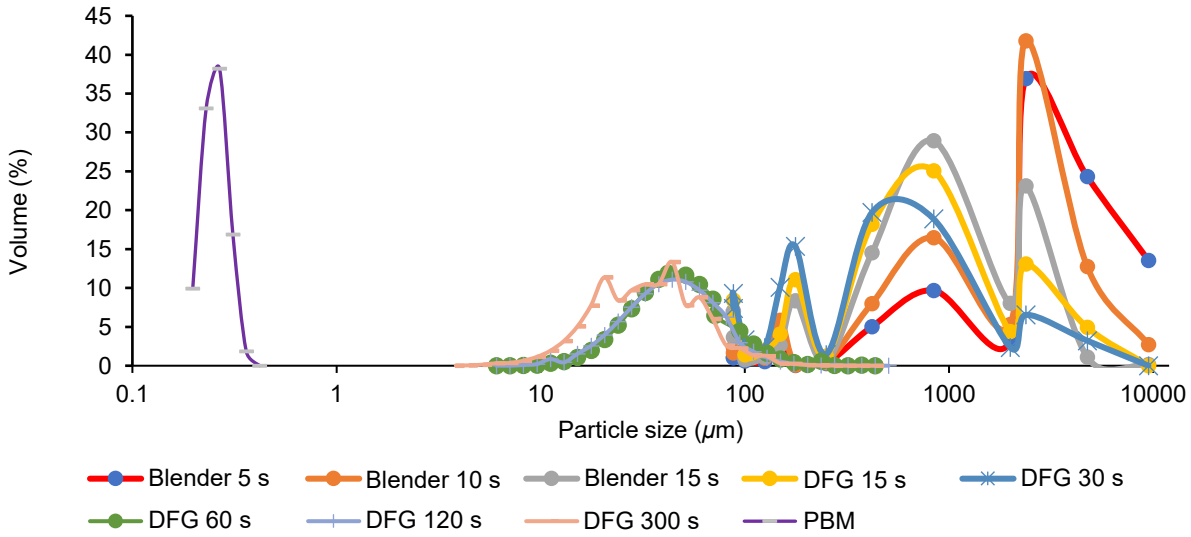

Figure 1. Particle size distribution of red ginger powder (RGP). Blender (5, 10, 15 s) and dry food grinder (DFG) 15 s samples were measured by sieve analysis, DFG (30, 60, 120, 300 s) samples by laser diffraction (LD), and planetary ball mill (PBM) sample, analyzed by dynamic light scattering (DLS) technique

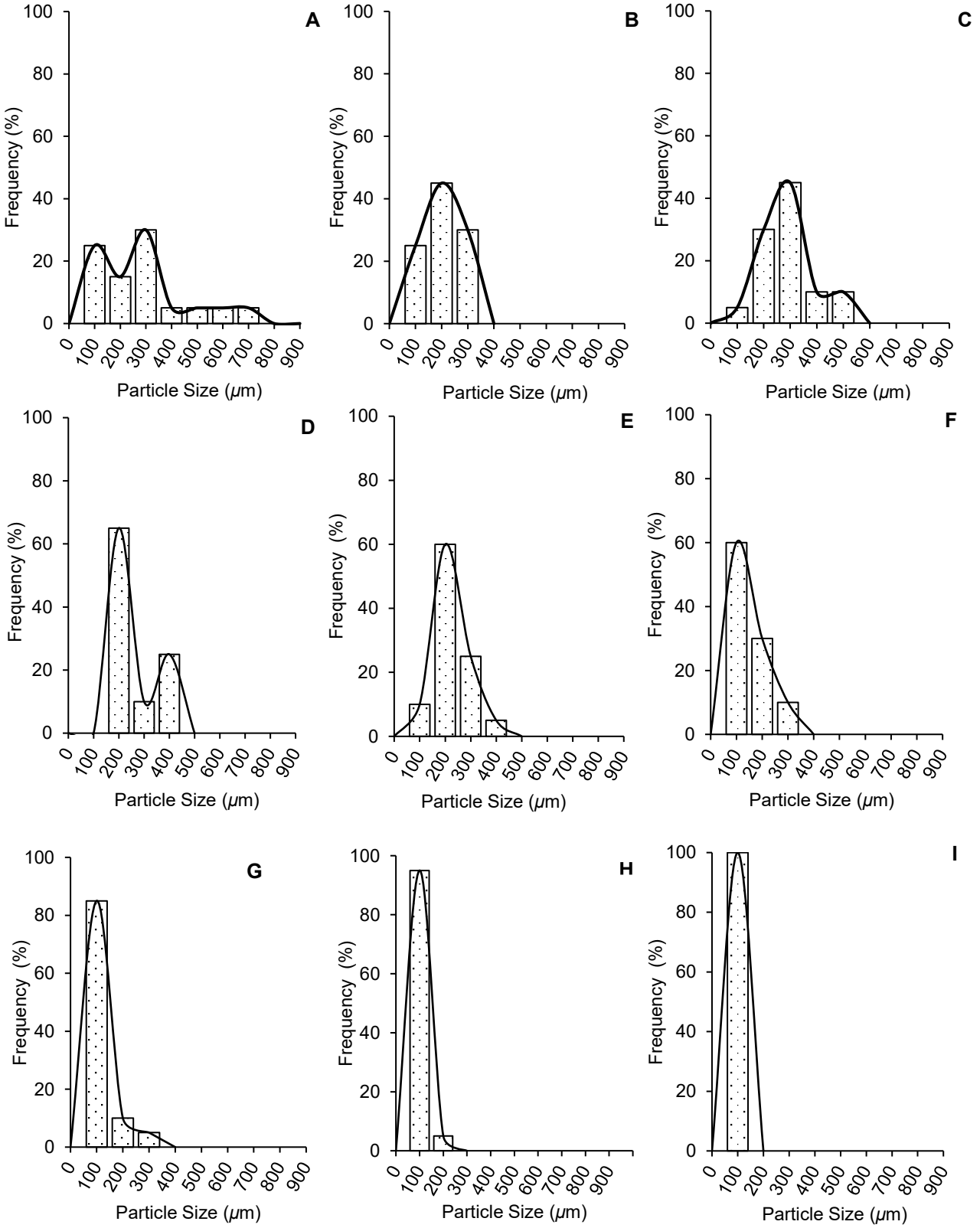

Note: Blender 5 s (A), 10 s (B), 15 s (C), DFG 15 s (D), 30 s (E), 60 s (F), 120 s (G), 300 s (H), PBM (I), DFG= dry food grinder, PBM= planetary ball mill

Figure 2. Particle size distribution of red ginger powder (RGP) based on particle diameter measured from scanning electron microscopy (SEM) images using ImageJ

The powder analyzed in this study exhibits irregular and asymmetric morphological characteristics. SEM was employed to visualize particle morphology and quantify particle dimensions based on the longest diameter. Although SEM can detect larger particles, it typically identifies them in limited quantities. DLS was used to analyze powders processed using the PBM. DLS is a non-invasive spectroscopic technique that determines particle-size distribution in liquid suspensions (generally within the 1–1000 nm range) by measuring fluctuations in scattered light intensity from nanoparticles (Jia *et al.,* 2023). Compared with SEM, DLS provides a more comprehensive assessment of size distribution because it analyzes a substantially larger number of particles.

It was confirmed that the particle size became smaller as the grinding time increased across the blender, DFG, and PBM methods. The powder was analyzed using the sieve, LD, and DLS methods and the results were compared with those obtained by the SEM. A consistent pattern was observed for all the parameters (D_{10}, D_{50}, D_{90}, and D_{av}), although the absolute values differed because sieving, laser diffraction, DLS, and SEM each report a different equivalent diameter. Laser diffraction reports a volume-weighted equivalent spherical diameter and is sensitive to particle shape and the optical model, which shifts the result towards sieving (which measures by mesh aperture) and SEM (which measures the longest 2-D length). This difference in measurement basis causes differences in particle size values between methods (Gorączko and Topoliński, 2020). Figures 1 and 2 show that the particle-size distribution decreased progressively from blender-ground to PBM-ground powder, indicating that finer grinding produced smaller and more homogeneous particles. Specifically, Figure 2 shows that the coarse powder produced by blender milling (D_{50} 2066–2256 μm) exhibits a broad size distribution, reflecting the heterogeneous distribution pattern typical of impact-based milling of fibrous plant materials (Zhao *et al.,* 2010). As the milling duration with DFG increases, the distribution becomes narrower, indicating a more uniform powder at finer particle sizes. Across all samples, D_{50} values obtained from SEM were consistently smaller than those obtained from sieve analysis but larger than those obtained from LD, which is due to the two-dimensional nature of SEM measurements and its limited field of view (Roostaei *et al.,* 2020; Whiting *et al.,* 2022), as discussed previously. The results from the various analytical were then used as a reference data for determining the particle size of the RGP.

Density

The density and flow characteristics of powder are crucial factors influencing their processing, packaging, and utilization in the industrial applications. Bulk density, tapped density, Hausner ratio, compressibility index, and angle of repose are common parameters to evaluate powder flowability (Carr, 1965). Table 2 shows the results of these measurements for RGP with different particle sizes (D_{50}).

As shown in Table 2, the bulk density of RGP does not follow a simple linear relationship with particle size reduction. The lowest bulk densities were recorded at D_{50} 39.98 and 40.37 μm (0.30±0.00 g/cm^3), which was significantly lower than the coarsest powder at D_{50} 2256 μm (0.32±0.00 g/cm^3) (p<0.05). This non-linear pattern is consistent with previous findings showing that superfine grinding does not always reduce bulk density. The relationship depends on changes in particle morphology, porosity, and interparticle void structure resulting from grinding (Huang *et al.,* 2018). Fine particles with irregular morphology tend to create larger interparticle voids, which can reduce bulk density, while further size reduction toward the nanoscale can improve packing efficiency as particles become more uniform (Duguma *et al.,* 2023).

The tapped density increased progressively and significantly with decreasing particle size (p<0.05), from 0.36±0.01 g/cm^3 at D_{50} 2256 μm to 0.56 ± 0.00 g/cm^3 at D_{50} 34.82 μm. This trend reflects the ability of smaller particles to rearrange more efficiently under mechanical tapping, thereby more effectively filling the interparticle voids (Huang *et al.,* 2018). It should be noted that the nanopowders (D_{50} 0.22 μm) did not show a significant difference in bulk density compared to the coarser DFG powder (D_{50} 39.98–40.37 μm), likely due to nanoparticle agglomeration reducing the effective packing efficiency during the compaction process.

Figures 3, 4, and Table 2 collectively show that particle size affects the flow characteristics of powders. Samples with larger particles (D_{50} between 2256 and 636 μm) exhibited low angle of repose (22.98–29.98°) and low Hausner ratio, indicating the very free flowing behavior. This means that larger particles experience weaker cohesive forces, which lowers the resistance to flow (Stavrou *et al.,* 2020). Conversely, smaller particles (D_{50} <50 μm) may exhibit either free or poor flowability. The angle of repose increases (32.26–36.95°), and both the Hausner ratio and compressibility index also increase. This trend indicates that smaller particles exhibit stronger interparticle forces such as van der Waals, capillary, and electrostatic forces due to the increased surface area (Fulchini *et al.,* 2017). Powder flowability at low stress is governed not by median size but also how wide the size distribution is and on the cohesive (van der Waals) forces between particles.

Table 2. Flow characteristics of red ginger powder (RGP)

D_{50} (μm)	Bulk Density (g/cm^3)	Tapped Density (g/cm^3)	Angle of Repose (°)	Flowability (Müller *et al.,* 2021)
2256	0.32±0.00^{bc}	0.36±0.01^{a}	22.98±0.01^{a}	very free flowing
2066	0.35±0.00^{de}	0.44±0.02^{b}	25.46±0.02^{b}	very free flowing
636	0.34±0.00^{d}	0.49±0.01^{de}	29.98±0.01^{de}	very free flowing
580	0.37±0.01^{f}	0.46±0.03^{c}	28.94±0.03^{c}	very free flowing
47.38	0.32±0.01^{b}	0.48±0.01^{cd}	32.26±0.01^{cd}	free flowing
40.37	0.30±0.02^{a}	0.51±0.00^{de}	36.95±0.00^{de}	free flowing
39.98	0.30±0.00^{a}	0.51±0.01^{e}	35.29±0.01^{e}	free flowing
34.82	0.34±0.01^{cd}	0.56±0.00^{f}	39.71±0.00^{f}	fair flowing
0.22	0.35±0.01^{ef}	0.56±0.02^{f}	37.07±0.02^{f}	free flowing

Note: Values are expressed as mean ± standard deviation (n= 3). Different superscript letters within the same column indicate significant differences (p<0.05) according to Duncan's multiple range test

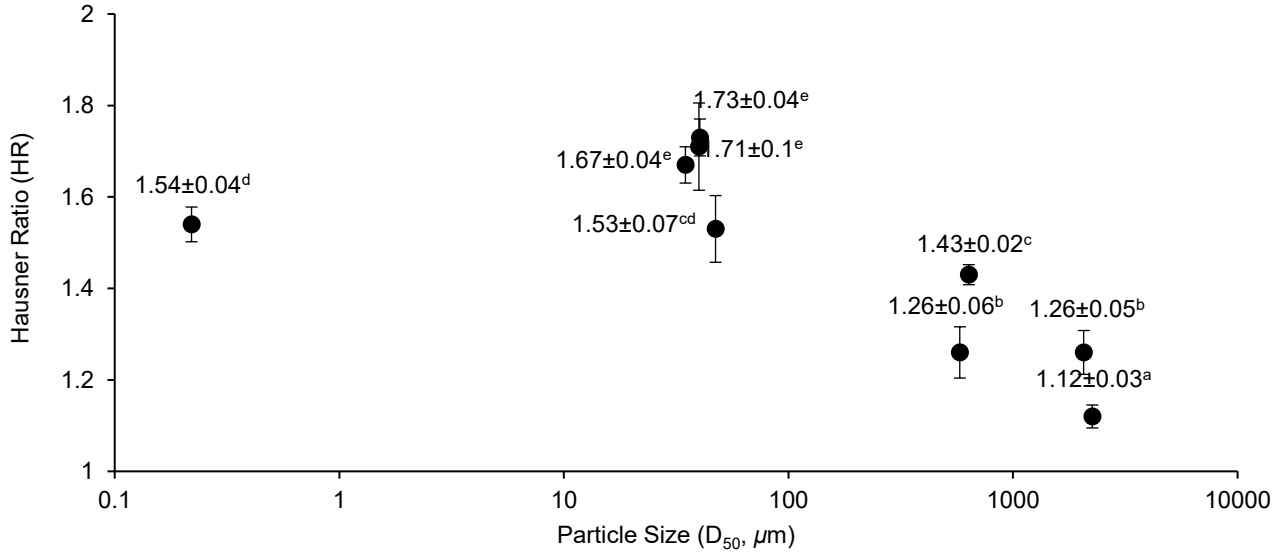

Figure 3. Relationship between particle size and Hausner ratio (HR). An increase in the Hausner ratio corresponds to a decrease in flowability, ranging from very free flow to very poor flow. Values are mean ± standard deviation

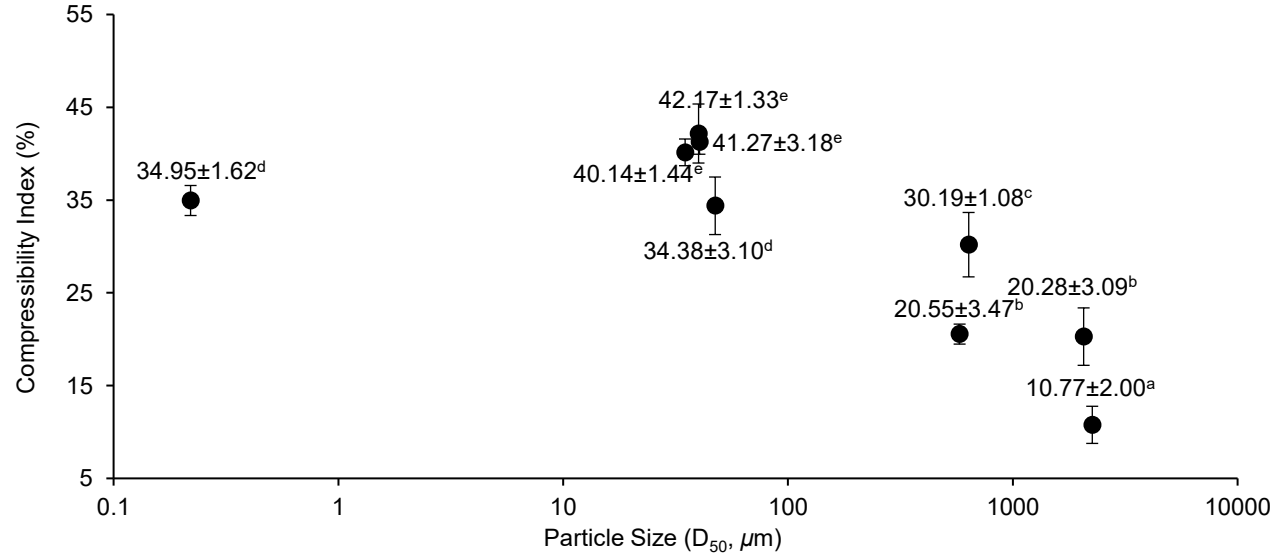

Figure 4. Relationship between particle size and compressibility index (%). An increase in compressibility index indicates a decrease in flowability, ranging from very free flow to very poor flow

As summarized in Table 1, the coarse blender-milled powder spanned a wide size range (D_{10} 344 μm; D_{90} 5963 μm; D_{50} 2256 μm), whereas the fine DFG-milled powder showed a much narrower distribution (D_{10} 18.10 μm, D_{90} 66.93 μm; D_{50} 34.82 μm). This narrower size distribution, together with the stronger interparticle van der Waals cohesion at finer sizes, reduces powder flowability (Stavrou *et al.,* 2020).

Flowability decreased as the Hausner ratio and compressibility index increased, as shown in Figures 3 and 4, indicating a transition from free-flowing to poor-flowing powder. Samples with larger particles (D_{50} between 2256 and 636 μm) exhibited low angle of repose (22.98–29.98°), classifying them as very free flowing according to Müller *et al.* (2021), consistent with weak cohesive forces at coarser particle sizes. Conversely, samples at D_{50} 47.38–40.37 μm (32.26–36.95°) were classified as free flowing, while D_{50} 34.82 μm (39.71°) fell into the fair flowing category, reflecting the increasing dominance of interparticle cohesive forces as particle size decreased (Müller *et al.,* 2021). Powders with particle sizes of 500–2000 μm generally showed good flowability due to a balance between gravitational and cohesive forces (Suhag *et al.,* 2024). Decreasing particle size has been associated with poorer flowability, as evidenced by increasing angle of repose, Hausner ratio, and compressibility index. This was statistically confirmed, as angle of repose differed significantly between treatments (p<0.05), increasing from 22.98±0.01° at D_{50} 2256 μm to 39.71±0.00° at D_{50} 34.82 μm. Samples at D_{50} 636 μm and D_{50} 47.38 μm did not show significant differences from each other, indicating a gradual transition in flowability at intermediate particle sizes.

When RGP was milled to the nanoscale (D_{50} 0.22 μm), the Hausner ratio, compressibility index, and angle of repose decreased slightly rather than increasing. This behavior is likely due to nanoparticle agglomeration, which reduces the accessible surface area or particle-particle contact area, resulting in improved flowability compared with micro powders (Suhag *et al.,* 2024). The angle of repose of the nanopowder (37.07±0.02°) was not significantly different from the D_{50} angle repose of 34.82 μm (39.71±0.00°), indicating that agglomeration at the nanoscale results in flow behavior comparable to that of fine micro powders.

Moisture content and water solubility

Moisture content refers to the total amount of water present in the powder (grams of water per gram of dry solid) (Juarez-Enriquez *et al.,* 2017). Solubility is defined as the concentration of solute in a saturated solution at a given temperature and depends on uniform molecular interactions within the system (Kumar and Singh, 2016). Particle size can influence both moisture retention and solubility, as shown in Figures 5 and 6.

The moisture content of RGP exhibits a non-linear relationship with particle size (D_{50}, μm). At larger particle sizes (>600 μm), moisture content remains relatively low (10–11%) with minimal variation among samples. A substantial increase is observed when particle size decreases to 40–50 μm, where moisture content reaches approximately 15%. Blender 15 s (D_{50} 580 μm) and DFG 15 s (D_{50} 636 μm), although produced by different milling methods, did not show significant differences in moisture content (10.98 and 10.89%, respectively) and water solubility (25.16 and 25.70%, respectively). This further supports the interpretation that particle size (D_{50}), rather than the milling method itself, played a major role in determining moisture content and water solubility in RGP. This increase is attributed to the larger specific surface area of smaller particles, which enhances exposure to the environment and promotes water adsorption through attractive interactions between water molecules and the particle surface.

Interestingly, when the particle size is reduced to the nanoscale (D_{50} 0.22 μm), the moisture content decreases again to 10.8%, showing no significant difference from that of the coarse powders. This behavior is likely due to particle agglomeration. Nanoparticles tend to cluster because of strong interparticle forces, effectively reducing the available surface area for water vapor adsorption (Yeap, 2018). As a result, agglomerated nanoscale particles may retain less moisture than fine microparticles.

RGP with a D_{50} of 0.22 μm exhibited the highest water solubility (31.65%), indicating that nanosizing enhances water solubility compared with microsized samples (Csicsák *et al.,* 2023). This relationship between specific surface area and solubility enhancement has been widely reported in the literature (Oti *et al.,* 2024). As shown in Figure 6, decreasing particle size corresponded with increased water solubility. Smaller particles possess a higher surface-area-to-volume ratio, enabling greater interaction with the solvent and thus improving solubility (Kumar and Singh, 2016). It should be noted that the relationship between particle size reduction and increased water solubility is not universally applicable to all food powder ingredients. In ingredients rich in hydrophobic components or crystalline starch, intensive milling may expose lipophilic groups that do not consistently improve solubility (Duguma *et al.,* 2023). Specifically, in RGP, the consistent increase in water solubility is further explained by two structural factors. First, progressive mechanical milling disrupts the ginger cell wall, exposing or releasing hydrophilic intracellular components, including soluble polysaccharides and other bioactive compounds such as gingerols that were previously inaccessible to solvents (Huang *et al.,* 2018).

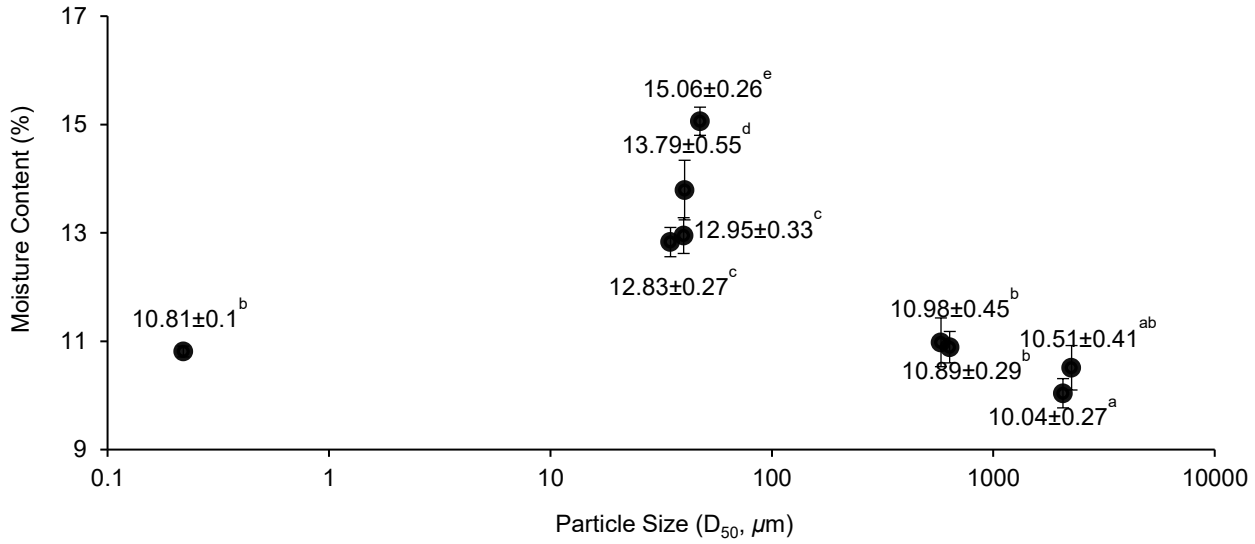

Figure 5. Relationship between particle size (D_{50}) and moisture content (%) of red ginger powder (RGP)

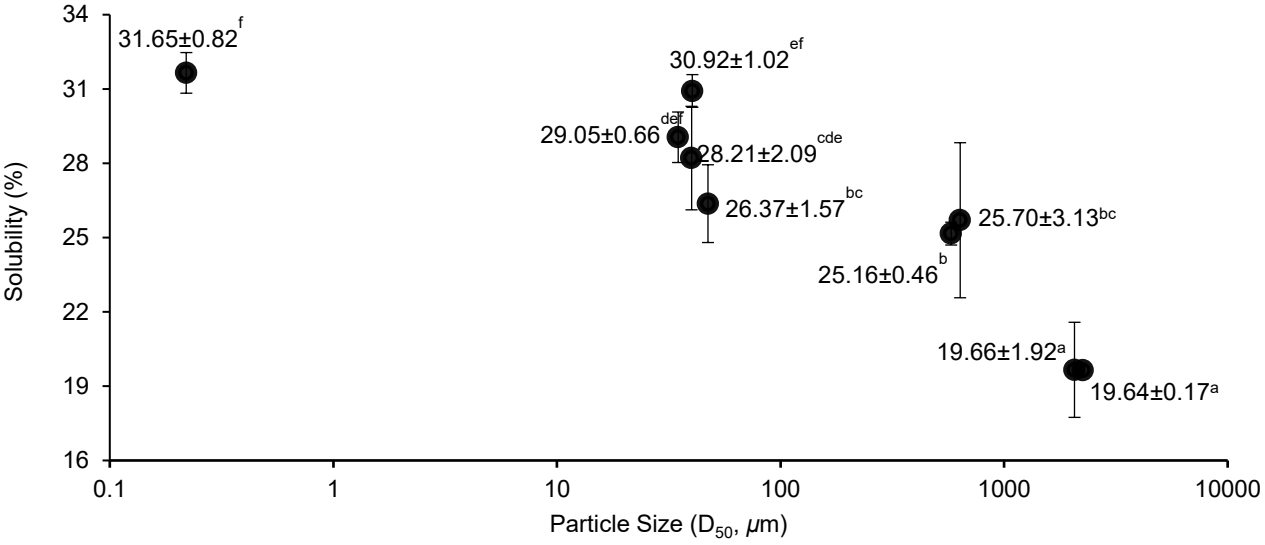

Figure 6. Relationship between particle size (D_{50}) and solubility (%) of red ginger powder (RGP)

Second, intensive milling, particularly through PBM, can induce partial amorphization of the starch and fiber fractions, reducing crystallinity and making previously less soluble components more water-dispersible (Xu *et al.,* 2021). Based on water solubility values, RGP with a D_{50} of 2256–34.82 μm can be categorized as water-soluble, whereas RGP with a D_{50} of 0.22 μm falls into the highly water-soluble category (Kumar and Singh, 2016). These functional-property gains follow the specific surface area and the exposure of inner cell-wall material as particles fracture; studies on spice-seed powders show solubility, color, and flow changing together as size is reduced (Oti *et al.,* 2024). Chemical profiles such as gingerols in dried ginger are suspected to be able to transform into shogaols under dry heat (Jung *et al.,* 2018), local heat, and mechanical stress from prolonged ball milling. Although chemical characterization is beyond the scope of this study.

Color

Color is an important quality attribute in food products and strongly influences consumer perception. Particle-size reduction has been shown to significantly affect powder color (Xu *et al.,* 2021). The color analysis results for RGP are presented in Table 3.

Based on Table 3, there is a statistically significant difference across all treatments (p<0.05), with L* increasing from 27.9±0.95 (D_{50} 2256 μm) to 55.4±0.72 (D_{50} 0.22 μm). For a* values, D_{50} 34.82 μm and 0.22 μm do not show significant differences from each other (p>0.05), indicating that extreme size reductions outside the micrometer range do not further increase redness.

Table 3. Characteristics of the color of red ginger powder (RGP)

D_{50} (μm)	L* Value	a* Value	b* Value	ΔE
2256	27.9±0.95^{a}	5.1±0.76^{a}	11.5±1.42^{a}	0.0±0.00^{a}
2066	29.5±2.81^{a}	7.1±1.27^{b}	17.8±1.11^{b}	7.4±0.21^{b}
636	35.9±1.03^{c}	7.7±1.14^{b}	19.3±1.81^{b}	11.6±0.21^{c}
580	32.4±0.72^{b}	7.5±1.53^{b}	19.1±1.14^{b}	9.4±0.18^{bc}
47.38	37.8±0.00^{c}	9.7±1.01^{c}	24.5±0.50^{c}	17.1±0.05^{d}
40.37	45.2±0.72^{e}	9.5±1.22^{c}	27.9±1.14^{d}	24.4±0.19^{e}
39.98	42.3±1.40^{d}	6.9±0.58^{b}	25.0±1.83^{c}	19.9±0.26^{d}
34.82	44.9±0.70^{e}	6.4±0.40^{ab}	25.7±1.14^{cd}	22.3±0.21^{e}
0.22	55.4±0.72^{f}	6.3±0.42^{ab}	26.8±0.80^{cd}	31.5±0.11^{f}

Note: Values are expressed as mean ± standard deviation (n= 3). Different superscript letters within the same column indicate significant differences (p<0.05) according to Duncan's multiple range test

Similarly, b* values at D_{50} 39.98 and 47.38 μm do not differ significantly (p>0.05), indicating a plateau in yellowness at intermediate fine particle sizes. ΔE increases significantly across all treatments, with nanopowder showing the largest color deviation from the reference sample (31.5±0.11). The findings indicate that decreasing particle size increases both L* (from 27.9 to 55.4) and ΔE (from 0.0 to 31.5), with ΔE calculated relative to the coarsest powder (D_{50} 2256 μm). Because the CIELAB values were obtained under a D_{50} illuminant and the CIE 1931 2° standard observer, with ΔE referenced to the coarsest powder (D_{50} 2256 μm), the large ΔE values of the fine and nanopowders (up to 31.5) represent color differences well above the threshold of visual perceptibility, confirming a visually distinct lightening of RGP with size reduction (Durmus, 2020). Milling induces internal structural changes, and smaller particles expose more internal components such as cellulose and hemicellulose. This increases light penetration and reflection, resulting in a brighter appearance (Huang *et al.,* 2018). Changes in the a* and b* coordinates were also observed: powders with D_{50} values of 2256–41 μm tended toward red (a*) and yellow (b*) hues, whereas samples with D_{50} values of 34.82 and 0.22 μm exhibited lower a* and b* values. The larger ΔE values of the fine powders (D_{50} 34.82 μm and 0.22 μm) indicate more pronounced color shifts relative to the coarse control (D_{50} 2256 μm). These results confirm that reducing particle size increases brightness and alters the red-yellow balance of RGP color. This trend aligns with previous findings showing that superfine grinding enhances the brightness of Tartar buckwheat powder (Xu *et al.,* 2021). Although all samples had the same drying history (50–55 °C for 40 h), which may affect ginger color (Nguyen *et al.,* 2026), the finer powders were also milled more intensively. This milling time generated varying amounts of heat. The measured color trends are likely due to both particle size and thermal and mechanical effects of milling. The visual appearance of RGP samples is shown in Figure 7.

As shown in Figure 7, the differences observed in powder appearance across milling treatments are consistent with the color analysis data in Table 3. The coarse powder produced by blender milling (D_{50} 2066–2256 μm) exhibited a darker, more reddish-brown appearance, consistent with the lower L* values (27.9–29.5) and higher a* and b* values observed in this size range. As particle size decreased to the micrometer range (D_{50} 34.82–47.38 μm), the powder appeared lighter and more yellowish, reflecting a significant increase in L* and ΔE values. Nanopowder (D_{50} 0.22 μm) exhibited the brightest and most uniform appearance among all samples, consistent with the highest L* value (55.4±0.72). These visible color differences have direct implications for consumer acceptance and product standardization, as color is one of the primary sensory attributes evaluated in spice powders (Oti *et al.,* 2024; Xu *et al.,* 2021). The gradual lightening of RGP with decreasing particle size suggests that milling intensity should be controlled to achieve the desired color profile for a given application.

Morphological analysis (SEM)

To further examine the morphological characteristics of RGP, SEM analysis was conducted on samples produced using different grinding methods and durations. The microstructural features of the powders are shown in Figure 8. SEM observations revealed clear changes in particle morphology as particle size decreased. Powders ground using a blender (D_{50} 2066–2256 μm) appeared as large, irregular aggregates with rough, non-uniform surfaces, indicating minimal structural breakdown of the ginger material.

When the particle size was reduced to D_{50} 580–636 μm, the powders displayed fragmented, irregular shapes with visible fibrous structures. In the medium particle-size range (D_{50} 34–47.38 μm), the particles appeared more homogeneous with a relatively uniform size distribution. At this scale, the increased surface area enhances interactions with the environment, consistent with increases in water solubility, moisture content, and other previously reported parameters. The morphological changes are thought to be due to mechanical damage to the ginger cell structure during the milling process. Powder ground

with a blender exhibits a rough and irregular surface, characteristic of cell wall fractures without significant internal structural damage. The fibrous structure seen at D_{50} 580–636 *μ*m indicates exposure of the plant's vascular tissue due to mechanical disturbance that has not completely broken down the cell wall (Zhao *et al.,* 2010). At finer particle sizes (D_{50} 34–47.38 *μ*m), a more homogeneous morphology indicates more thorough cell wall damage and the release of intracellular hydrophilic components such as starch and soluble polysaccharides (Duguma *et al.,* 2023). At the nanoscale (D_{50} 0.22 *μ*m), the powder exhibited a much smoother and more uniform morphology. However, notable agglomeration was observed, where nanoparticles clustered into aggregates. Such behavior is common in nanosized powders due to strong interparticle forces (e.g., van der Waals and electromagnetic interactions), which effectively reduce the accessible surface area (Yeap, 2018). This explains the lower-than-expected moisture content of the nanopowder and its improved flow properties compared with microparticles.

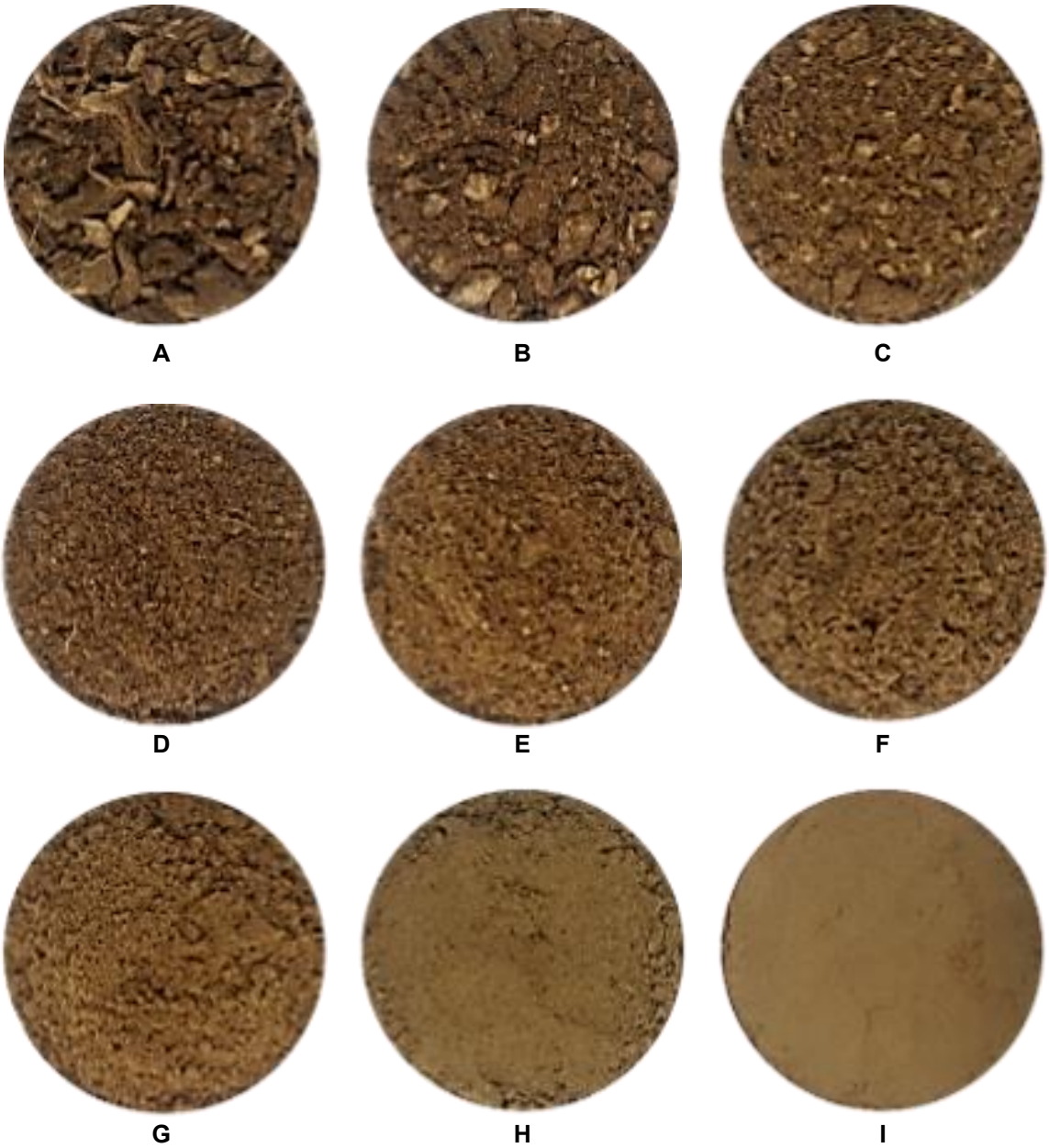

Note: Particle sizes in *μ*m= 2256 (A), 2066 (B), 580 (C), 636 (D), 47.38 (E), 39.98 (F), 40.37 (G), 34.82 (H), 0.22 (I)

Figure 7. Appearance of red ginger powder (RGP) with various particle sizes

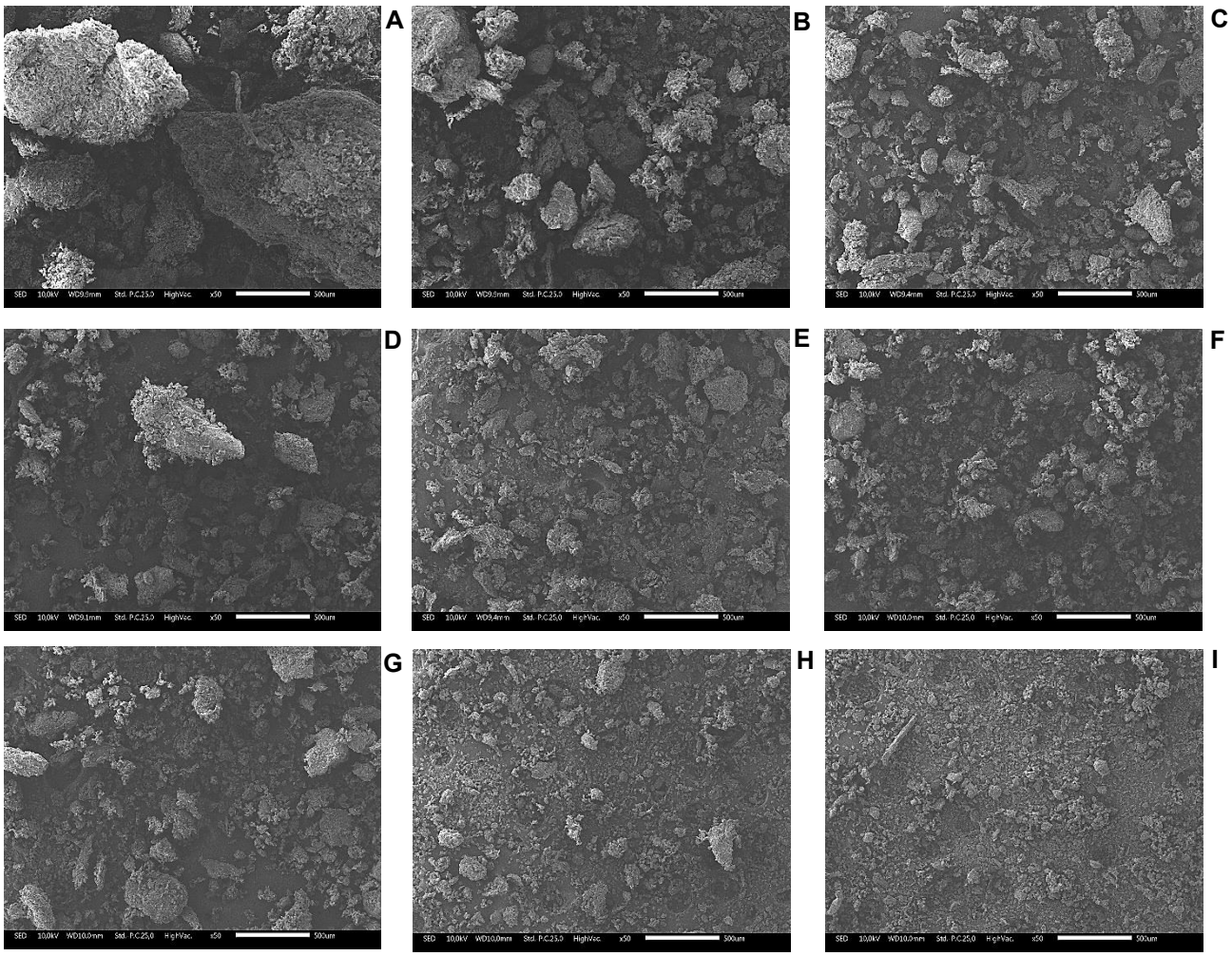

Note: D_{50} (μm)= 2256 (A), 2066 (B), 636 (C), 580 (D), 47.38 (E), 39.98 (F), 40.37 (G), 34.82 (H), 0.22 (I)

Figure 8. Appearance of red ginger powder (RGP) with SEM operated at 20 kV, 50× magnification

CONCLUSION

Particle size reduction significantly affected the physical properties of RGP across the millimeter, micrometer, and nanometer size ranges evaluated in this study. Particle size reduction from the millimeter to micrometer scale resulted in an increase in tapped density and water solubility, whereas bulk density showed a non-linear trend. However, there was a decrease in powder flowability as indicated by increase of Hausner ratio, compressibility index, and angle of repose, indicating a shift from highly flowable to moderately flowable behavior. At the nanoscale (D_{50} 0.22 μm), a different pattern emerged: flowability increased slightly relative to fine micrometer-sized powder, moisture content decreased, and solubility and brightness reached their highest observed values. This nanoscale behavior is primarily due to particle agglomeration driven by strong interparticle forces. The behavior of nanoscale powders in this study is based on a single PBM condition; broader conclusions at this scale require further investigation across a wider range of nanoscale particle sizes. Overall, these findings suggest that particle size reduction offers a practical approach to tailoring the physical properties of RGP for specific food applications, although the optimal size range will depend on the targeted properties and intended use.

ACKNOWLEDGMENT

This research was funded by the Indonesian Education Scholarship from the Ministry of Education, Culture, Research, and Technology; the Center for Financing and Assessment of Higher Education (PPAPT); and the Education Fund Management Institute (BPI ID: 202101120991).

REFERENCES

Abel, S. E. R., Yusof, Y. A., Chin, N. L., Chang, L. S., Ghazali, H. M., & Manaf, Y. N. (2020). Characterization of physicochemical properties of gum arabic powder at various particle sizes. *Food Research*, *4*(Suppl. 1), 107–115. https://doi.org/10.26656/fr.2017.4(S1).S32

Badrunanto, Wahyuni, W. T., Farid, M., Batubara, I., & Yamauchi, K. (2024). Antioxidant components of the three different varieties of Indonesian ginger essential oil: In vitro and computational studies. *Food Chemistry Advances*, *4*, 100558. https://doi.org/10.1016/j.focha.2023.100558

Biazzi, H. M., Tubin, J. S. B., Conte, R. A., Robazza, W. da S., & Paiano, D. (2022). Different sieving methods for determining the physical characteristics in ground corn. *Acta Scientiarum, Animal Sciences*, *44*, e53382. https://doi.org/10.4025/actascianimsci.v44i1.53382

Camacho, M. M., Silva-Espinoza, M. A., & Martínez-Navarrete, N. (2022). Flowability, rehydration behaviour and bioactive compounds of an orange powder product as affected by particle size. *Food and Bioprocess Technology*, *15*, 683–692. https://doi.org/10.1007/s11947-022-02773-9

Cano-Chauca, M., Stringheta, P. C., Ramos, A. M., & Cal-Vidal, J. (2005). Effect of the carriers on the microstructure of mango powder obtained by spray drying and its functional characterization. *Innovative Food Science and Emerging Technologies*, *6*(4), 420–428. https://doi.org/10.1016/j.ifset.2005.05.003

Carr, R. L. (1965). Evaluating flow properties of solids. *Chemical Engineering*, *72*, 163–168. https://doi.org/10.1001/archopht.1965.00970040165007

Csicsák, D., Szolláth, R., Kádár, S., Ambrus, R., Bartos, C., Balogh, E., Antal, I., Köteles, I., Tőzsér, P., Bárdos, V., Horváth, P., Borbás, E., Takács-Novák, K., Sinkó, B., & Völgyi, G. (2023). The effect of the particle size reduction on the biorelevant solubility and dissolution of poorly soluble drugs with different acid-base character. *Pharmaceutics*, *15*(1). 278. https://doi.org/10.3390/pharmaceutics15010278

Dacanal, G. C. (2024). Particle size and morphology in food science and technology: A review. *International Journal of Food Science and Technology*, *59*(10), 6821–6833. https://doi.org/10.1111/ijfs.17475

Duguma, H. T., Zhang, L., Ofoedu, C. E., Chacha, J. S., & Agunbiade, A. O. (2023). Potentials of superfine grinding in quality modification of food powders. *CyTA - Journal of Food, 21*(1), 530–541. https://doi.org/10.1080/19476337.2023.2249068

Durmus, D. (2020). CIELAB color space boundaries under theoretical spectra and 99 test color samples. *Color Research & Application*, *45*(5), 796–802. https://doi.org/10.1002/col.22521

Fulchini, F, Zafar, U., Hare, C., Ghadiri, M., Tantawy, H., Ahmadian, H., Poletto, M. (2017). Relationship between surface area coverage of flow-aids and flowability of cohesive particles. *Powder Technology*, *322*, 417–427. https://doi.org/10.1016/j.powtec.2017.09.013

Gorączko, A., & Topoliński, S. (2020). Particle size distribution of natural clayey soils: A discussion on the use of laser diffraction analysis (LDA). *Geosciences*, *10*(2), 55. https://doi.org/10.3390/geosciences10020055

Hausner, H. H. (1967). Friction condition in a mass of metal powder. *International Journal of Powder Metallurgy, 3*(4)*,* 7–13.

Huang, X., Dou, J.-Y., Li, D., & Wang, L.-J. (2018). Effects of superfine grinding on properties of sugar beet pulp powders. *LWT*, *87*, 203–209. https://doi.org/10.1016/j.lwt.2017.08.067

Islam, S. F., Hawkins, S. M., Meyer, J. L. L., & Sharman, A. R. C. (2022). Evaluation of different particle size distribution and morphology characterization techniques. *Additive Manufacturing Letters*, *3*, 1000077. https://doi.org/10.1016/j.addlet.2022.100077

Jia, Z., Li, J., Gao, L., Yang, D., & Kanaev, A. (2023). Dynamic light scattering: A powerful tool for in situ nanoparticle sizing. *Colloids and Interfaces*, *7*(1), 15. https://doi.org/10.3390/colloids7010015

Juarez-Enriquez, E., Olivas, G. I., Zamudio-Flores, P. B., Ortega-Rivas, E., Perez-Vega, S., & Sepulveda, D. R. (2017). Effect of water content on the flowability of hygroscopic powders. *Journal of Food Engineering*, *205*, 12–17. https://doi.org/10.1016/j.jfoodeng.2017.02.024

Jung, M. Y., Lee, M. K., Park, H. J., Oh, E.-B., Shin, J. Y., Park, J. S., Jung, S. Y., Oh, J.-H., & Choi, D.-S. (2018). Heat-induced conversion of gingerols to shogaols in ginger as affected by heat type (dry or moist heat), sample type (fresh or dried), temperature and time. *Food Science and Biotechnology*, *27*, 687–693. https://doi.org/10.1007/s10068-017-0301-1

Kumar, S., & Singh, P. (2016). Various techniques for solubility enhancement: An overview. *The Pharma Innovation Journal*, *5*(1), 23–28.

Mao, Q.-Q., Xu, X.-Y., Cao, S.-Y., Gan, R.-Y., Corke, H., Beta, T., & Li, H.-B. (2019). Bioactive compounds and bioactivities of ginger (*Zingiber officinale* Roscoe). *Foods*, *8*(6), 185. https://doi.org/10.3390/foods8060185

Müller, D., Fimbinger, E., & Brand, C. (2021). Algorithm for the determination of the angle of repose in bulk material analysis. *Powder Technology*, *383*, 598–605. https://doi.org/10.1016/j.powtec.2021.01.010

Nguyen, N. H. K., Tran, N. Q., Nguyen, L. T. N., Nguyen, N. T., & Huynh, Q. P. (2026). Effect of drying methods on the quality of ginger powder and its application in functional gummy candy. *International Journal of Food Science*, *2026*(1), 442059. https://doi.org/10.1155/ijfo/4442059

Oti, H. C., Offia-Olua, B. I., & Ukom, A. N. (2024). Flavour profiles, antioxidant activity, particle size distribution and functional properties of some ethnic spice seed powder used as food additive. *Food Chemistry Advances*, *5*, 100744. https://doi.org/10.1016/j.focha.2024.100744

Permanadewi, I., Kumoro, A. C., Wardhani, D. H., & Aryanti, N. (2022). Effect of viscosity on iron encapsulation using alginate as a carrying agent in a controlled spray drying process. *Food Research*, *6*(5), 56–67. https://doi.org/10.26656/fr.2017.6(5).613

Roostaei, M., Hosseini, S. A., Soroush, M., Velayati, A., Alkouh, A., Mahmoudi, M., Ghalambor, A., & Fattahpour, V. (2020). Comparison of various particle-size distribution-measurement methods. *SPE Reservoir Evaluation and Engineering*, *23*(4), 1159–1179. https://doi.org/10.2118/199335-PA

Shen, L., Li, Q. Q., Kang, Y. H., Xiang, Q. Q., Luo, X., & Chen, L. Q. (2023). Metabolomics reveals size-dependent persistence and reversibility of silver nanoparticles toxicity in freshwater algae. *Aquatic Toxicology*, *258*, 106471. https://doi.org/10.1016/j.aquatox.2023.106471

Stavrou, A. G., Hare, C., Hassanpour, A., & Wu, C.-Y. (2020). Investigation of powder flowability at low stresses: Influence of particle size and size distribution. *Powder Technology*, *364*, 313–323. https://doi.org/10.1016/j.powtec.2020.01.068

Suhag, R., Kellil, A., & Razem, M. (2024). Factors influencing food powder flowability. *Powders*, *3*(1), 65–76. https://doi.org/10.3390/powders3010006

Weston, M., Phan, M. A. T., Arcot, J., & Chandrawati, R. (2020). Anthocyanin-based sensors derived from food waste as an active use-by date indicator for milk. *Food Chemistry*, *326*, 127017. https://doi.org/10.1016/j.foodchem.2020.127017

Whiting, J. G., Garboczi, E. J., Tondare, V. N., Scott, J. H. J., Donmez, M. A., & Moylan, S. P. (2022). A comparison of particle size distribution and morphology data acquired using lab-based and commercially available techniques: Application to stainless steel powder. *Powder Technology*, *396*, 648–662. https://doi.org/10.1016/j.powtec.2021.10.063

Xu, Q., Zheng, F., Cao, X., Yang, P., Xing, Y., Zhang, P., Liu, H., Zhou, G., Liu, X., & Bi, X. (2021). Effects of airflow ultrafine-grinding on the physicochemical characteristics of tartary buckwheat powder. *Molecules*, *26*(19), 5481. https://doi.org/10.3390/molecules26195841

Yeap, S. P. (2018). Permanent agglomerates in powdered nanoparticles: Formation and future prospects. *Powder Technology*, *323*, 51–59. https://doi.org/10.1016/j.powtec.2017.09.042

Zhao, X., Ao, Q., Du, F., Zhu, J., & Liu, J. (2010). Surface characterization of ginger powder examined by X-ray photoelectron spectroscopy and scanning electron microscopy. *Colloids and Surfaces B: Biointerfaces*, *79*(2), 494–500. https://doi.org/10.1016/j.colsurfb.2010.05.019